

ELECTRON CAPTURES ON ¹⁴N AS A TRIGGER FOR HELIUM SHELL DETONATIONS

EVAN B. BAUER,¹ JOSIAH SCHWAB,^{2,*} AND LARS BILDSTEN^{1,3}

¹*Department of Physics, University of California, Santa Barbara, CA 93106, USA*

²*Department of Astronomy and Astrophysics, University of California, Santa Cruz, CA 95064, USA*

³*Kavli Institute for Theoretical Physics, University of California, Santa Barbara, CA 93106, USA*

(Received May 15, 2017; Revised July 10, 2017; Accepted July 13, 2017)

Submitted to The Astrophysical Journal

ABSTRACT

White dwarfs (WDs) that accrete helium at rates $\sim 10^{-8} M_{\odot} \text{yr}^{-1}$, such as those in close binaries with sdB stars, can accumulate large ($\gtrsim 0.1 M_{\odot}$) helium envelopes which are likely to detonate. We perform binary stellar evolution calculations of sdB+WD binary systems with MESA, incorporating the important reaction chain $^{14}\text{N}(e^{-}, \nu)^{14}\text{C}(\alpha, \gamma)^{18}\text{O}$ (NCO), including a recent measurement for the $^{14}\text{C}(\alpha, \gamma)^{18}\text{O}$ rate. In large accreted helium shells, the NCO reaction chain leads to ignitions at the dense base of the freshly accreted envelope, in contrast to 3α ignitions which occur away from the base of the shell. In addition, at these accretion rates, the shells accumulate on a timescale comparable to their thermal time, leading to an enhanced sensitivity of the outcome on the accretion rate history. Hence, time dependent accretion rates from binary stellar evolution are necessary to determine the helium layer mass at ignition. We model the observed sdB+WD system CD $-30^{\circ}11223$ and find that the inclusion of these effects predicts ignition of a $0.153 M_{\odot}$ helium shell, nearly a factor of two larger than previous predictions. A shell with this mass will ignite dynamically, a necessary condition for a helium shell detonation.

Keywords: white dwarfs – supernovae: general – binaries: close – novae, cataclysmic variables – nuclear reactions, abundances

1. INTRODUCTION

Many accreting white dwarfs (WDs) are discovered when a thermonuclear instability (i.e. nova) occurs on their surface. These outcomes depend on the accreting fuel, the accretion rate, \dot{M} , and the WD mass. The growing AM CVn class of binaries are WDs accreting from a Roche lobe filling helium donor (Nelemans et al. 2004). No hydrogen is seen. Recent observations are beginning to unveil one possible class of progenitors for these systems, tight sdB+WD binaries ($P_{\text{orb}} < 100$ min) that should make contact within the sdB star’s helium burning lifetime (Geier et al. 2013; Kupfer et al. 2017). Due to the large He shells that are likely to accumulate prior to the onset of the initial thermonuclear instability, such systems are of interest as potential environments for helium detonations that can lead to “Ia” supernovae or even double detonation supernovae (Nomoto 1982; Woosley & Weaver 1994; Bildsten et al. 2007; Shen & Bildsten 2009, 2014; Woosley & Kasen 2011; Brooks et al. 2015).

When accreting from the outer, unburned layers of a He burning star, the isotope ^{14}N is present with a mass fraction set by the initial stellar metallicity, $X_{14} \approx 0.01(Z/0.02)$. When the accretor is a WD, this ^{14}N is an important isotope, as it captures an electron when densities above $1.25 \times 10^6 \text{ g cm}^{-3}$ are reached. The resulting ^{14}C then undergoes the reaction $^{14}\text{C}(\alpha, \gamma)^{18}\text{O}$ that can trigger a thermonuclear flash (Hashimoto et al. 1986). This process, known as the NCO chain, requires the accumulation of a dense shell prior to the initiation of any thermonuclear instability, and is the subject of our study.

Hashimoto et al. (1986) showed that this reaction chain can lead to an earlier ignition than expected from the 3α reaction alone when accreting He onto a He WD, and Iben et al. (1987) and Shen & Bildsten (2009) noted its potential importance for accretion onto C/O WDs. Woosley & Weaver (1994) included the NCO chain in their models of sub-Chandrasekhar helium detonations. Piersanti et al. (2001) discussed the influence of NCO burning on the location of the ignition point for large, degenerate He envelopes on C/O WDs formed at constant $\dot{M} \approx 10^{-8} M_{\odot} \text{ yr}^{-1}$. They concluded that NCO burning only marginally decreased accumulated He layer mass, and noted that NCO burning did not lift degeneracy and prevent instability. Woosley & Kasen (2011) highlighted the role of the NCO chain in their survey of C/O WDs accreting He at $\dot{M} = (1 - 10) \times 10^{-8} M_{\odot} \text{ yr}^{-1}$, finding that the electron captures modify the neutron excess of the burned material and reduce the density at which the thermonuclear runaway initiates. This \dot{M} and WD mass regime

is coincident with that realized in the sdB donor star scenario (Iben et al. 1987; Brooks et al. 2015) and so needs a thorough investigation.

Our exploration of NCO ignitions in accreted He envelopes on C/O WDs using MESA confirms the importance of the NCO chain for systems accreting at rates corresponding to sdB+WD scenarios. Section 2 describes the relevant reaction rates used as input for MESA, relying on the recent work of Paxton et al. (2015) and Schwab et al. (2015) for the electron capture physics and Johnson et al. (2009) for α captures on ^{14}C . Section 3 shows MESA results for models at constant \dot{M} to explore broad trends in the influence of the NCO chain. Section 4 shows MESA results that include binary evolution with resulting variable accretion rates. These binary results are qualitatively different from what is found at constant \dot{M} , demonstrating the importance of self-consistent evolution coupling detailed binary evolution and accretion histories to modeling of the accreting WD up to ignition of the He. The system CD $-30^{\circ}11223$ (Geier et al. 2013) serves as a case study that naturally illustrates the importance of models including both NCO reactions and realistic binary accretion histories.

2. THE NCO REACTION CHAIN

Unless otherwise specified, all modeling presented in this work relies on MESA version r8118 with reaction networks including weak reactions between ^{14}N and ^{14}C as well as α -capture onto ^{14}C . This section describes the details of the rates for these reactions, which together make up the complete NCO chain.

2.1. Weak Reactions for ^{14}N and ^{14}C

Tabulated rates for the electron-capture and beta-decay reactions linking ^{14}N and ^{14}C are not included in MESA version r8118. In order to incorporate these important rates, we used a modified version of MESA’s on-the-fly weak reaction rate capabilities¹ (Paxton et al. 2015; Schwab et al. 2015; Paxton et al. 2016; Schwab et al. 2016). The rate of interest is that of the ground state ($^{14}\text{N} : J^{\pi} = 1^{+}$) to ground state ($^{14}\text{C} : J^{\pi} = 0^{+}$) transition. This has a Q -value of 0.1565 MeV, corresponding to a threshold density of $\rho_{\text{th}} = 1.156 \times 10^6 \text{ g cm}^{-3}$ for electron fraction $Y_e = 0.5$. The ft -value for ^{14}C beta decay is $\log(ft/s) = 9.04$ (Ajzenberg-Selove 1991), with the ft -value for electron capture being a factor of 3 lower, corresponding to the ratio of the spin degeneracies $(2J_{\text{N}} + 1)/(2J_{\text{C}} + 1)$.

¹ Our inlists and patches for MESA r8118 will be made available at <http://mesastar.org>.

The previous application of these capabilities (Schwab et al. 2015; Martínez-Rodríguez et al. 2016) focused on the high-density regime where the degenerate electrons are ultra-relativistic, and therefore we must make one slight modification to the treatment included in MESA version r8118. The equations implemented assume that G , the Coulomb barrier factor, can be approximated as a constant and thus removed from the phase space integral. This is true in the ultra-relativistic regime, where $G = \exp(\pi\alpha Z) \approx 1.2$ as well as in the non-relativistic regime, where $G = 2\pi\alpha Z \approx 0.32$ (Fuller et al. 1980). However, the density where the electron Fermi energy $E_F \approx m_e c^2$ is $\rho \approx 2 \times 10^6 \text{ g cm}^{-3}$ (for $Y_e = 0.5$), near ρ_{th} . We are not in either limiting regime. Fuller et al. (1985) remove G from the integral by replacing it with a suitably defined average value, $\langle G \rangle$. These values vary with density and temperature; however, we find the choice of a single average value $\langle G_\beta \rangle = 0.75$ (for beta decay) and $\langle G_{\text{ec}} \rangle = 0.95$ (for electron capture) reproduces the rates calculated without removing G from the integral to within $\approx 10\%$ over the regime of interest ($5 \leq \log(\rho/\text{g cm}^{-3}) \leq 7$ and $7 \leq \log(T/\text{K}) \leq 9$).

Figure 1 shows these weak reaction rates. We confirmed that these rates agree with the rates in Hashimoto et al. (1986) to within $\approx 10\%$ at the relevant, near-threshold densities. The work of Woosley & Kasen (2011) used the Hashimoto et al. (1986) results. As discussed by Hashimoto et al. (1986), the most important aspect of these rates is the shift in equilibrium composition from ^{14}N (at $\rho < \rho_{\text{th}}$) to ^{14}C (at $\rho > \rho_{\text{th}}$) over a narrow range in density $\Delta \log \rho \approx (k_B T)/E_F$.

The rates in our MESA calculations include an additional correction not present in the rates shown in Figure 1; this ‘‘ion Coulomb correction’’ corresponds to the energetic cost to change the ion charge in the dense plasma. We evaluate the magnitude of this effect using the ion chemical potential from Potekhin et al. (2009). At the densities and temperatures of interest, this energy difference is $\Delta\mu_{\text{ion}} \approx 7 \text{ keV}$. This corresponds to an increase of the threshold density by $\Delta\rho_{\text{th}} \approx 10^5 \text{ g cm}^{-3}$. When referring to the threshold density for our MESA models, we use the value $\rho_{\text{th}} = 1.25 \times 10^6 \text{ g cm}^{-3}$ which accounts for this correction.

2.2. The $^{14}\text{C}(\alpha, \gamma)^{18}\text{O}$ Rate

Historically, the $^{14}\text{C}(\alpha, \gamma)^{18}\text{O}$ rate has been uncertain by several orders of magnitude due to a poorly constrained, near-threshold, 3^- resonance in ^{18}O at 6.404 MeV, which dominates the rate for temperatures $3 \times 10^7 \text{ K} < T < 3 \times 10^8 \text{ K}$. Figure 2 shows the rate given in equation (1) of Hashimoto et al. (1986), as well as the rate from Iliadis et al. (2010), via the JINA Rea-

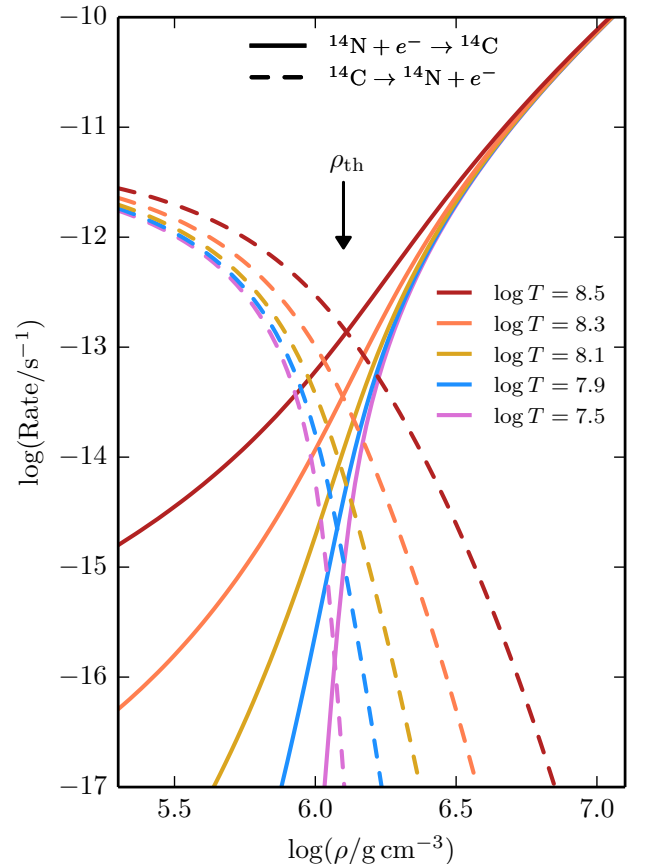


Figure 1. Rates for electron-capture and beta-decay reactions linking ^{14}N and ^{14}C (for $Y_e = 0.5$). So as to compare with previous work, this plot neglects the Coulomb correction.

lib database (Cyburt et al. 2010), that was adopted as the default rate in MESA (Paxton et al. 2011, 2013). The contrast between these rates illustrates the large historical uncertainty associated with the temperature regime dominated by the resonance.

For this work we use the measurements of Johnson et al. (2009) for the temperature regime $T > 3 \times 10^7 \text{ K}$, where the rate is dominated by the 3^- and 4^+ resonances. We have adopted the rates given in their equation (12) for those resonances, with a claimed uncertainty of just 35% for the 3^- resonance. Thus, the historical uncertainty associated with the $^{14}\text{C}(\alpha, \gamma)^{18}\text{O}$ rate is now greatly reduced in the temperature regime relevant for our problem. The contributions from these resonances are plotted in Figure 2 for comparison to the other full rates. For lower temperatures where these resonances do not dominate, we switch back to using the rate from Iliadis et al. (2010) for simplicity, though the rate is so small in this region that it will not be sig-

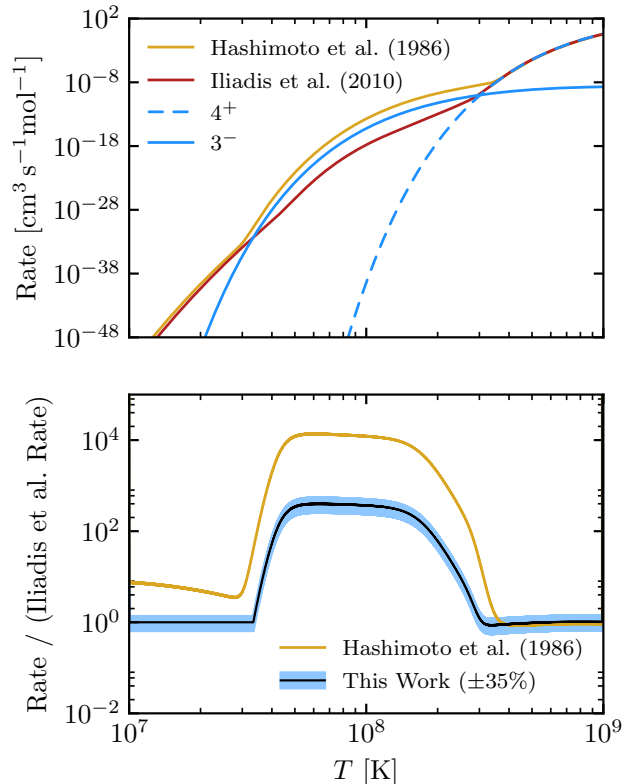


Figure 2. (Top) The $^{14}\text{C}(\alpha, \gamma)^{18}\text{O}$ rates from Hashimoto et al. (1986) and Iliadis et al. (2010), along with the specific resonances that dominate for $T > 3 \times 10^7$ K as measured by Johnson et al. (2009). (Bottom) The $^{14}\text{C}(\alpha, \gamma)^{18}\text{O}$ rates from this work and Hashimoto et al. (1986) relative to the rate from Iliadis et al. (2010).

nificant. The lower panel of Figure 2 shows the total resulting rate that we have adopted for this work relative to the default rate found in MESA version r8118 from Iliadis et al. (2010).

2.3. Example of He Accretion onto a He WD

To exhibit how MESA compares to prior work, we used MESA to reproduce the He WD evolution scenarios described in section 4 and figure 5 of Hashimoto et al. (1986). A $0.3 M_{\odot}$ He WD model accretes He until the center is compressed and heated enough to undergo an NCO induced thermonuclear runaway. In Figure 3, we compare cases with different rates for the $^{14}\text{C}(\alpha, \gamma)^{18}\text{O}$ step in the NCO chain, as well as a case where NCO reactions are omitted from the network. For higher accretion rates, the temperature of the core is high enough that electron captures are the rate limiting step for the NCO chain, and hence we see no difference in the evolution tracks when using different $^{14}\text{C}(\alpha, \gamma)^{18}\text{O}$ rates. For lower accretion rates, however, the core evolution

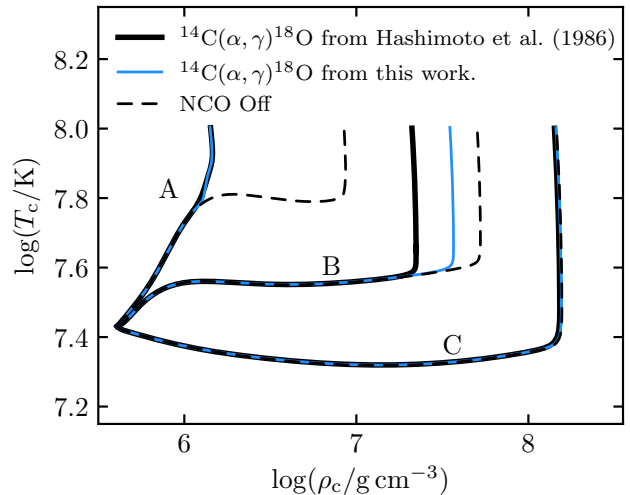


Figure 3. MESA models of He accretion onto a He WD reproducing those shown by figure 5 in Hashimoto et al. (1986). Solid black lines show core ignition via the NCO chain using the $^{14}\text{C}(\alpha, \gamma)^{18}\text{O}$ rate given by Hashimoto et al. (1986) equation (1). Dashed lines show ignition when NCO burning is ignored and only 3α plays a role. Solid blue lines show the result from NCO ignition using the $^{14}\text{C}(\alpha, \gamma)^{18}\text{O}$ rate described in Section 2.2 of this work. The three different cases are constant He accretion rates of (A) $10^{-8} M_{\odot} \text{yr}^{-1}$, (B) $10^{-9} M_{\odot} \text{yr}^{-1}$, and (C) $3 \times 10^{-10} M_{\odot} \text{yr}^{-1}$.

tracks reach well beyond the threshold density for electron captures, so that electron captures are no longer the rate limiting step for the NCO chain. Instead, the tracks lie in a temperature region where ^{14}C burning dominates the net NCO rate, and we see that the improved $^{14}\text{C}(\alpha, \gamma)^{18}\text{O}$ rate (Johnson et al. 2009) substantially changes the final outcome for case B. In case C, He burning triggers the thermonuclear runaway before NCO has a chance, so the $^{14}\text{C}(\alpha, \gamma)^{18}\text{O}$ rate ends up being irrelevant for igniting the flash.

3. NCO REACTIONS AND HELIUM ACCRETION

Due to the steep density dependence of the electron capture rates, we expect the NCO chain to play a significant role only when the density at the base of an accreted He shell reaches values above the threshold density of $\rho_{\text{th}} = 1.25 \times 10^6 \text{g cm}^{-3}$ prior to thermonuclear ignition. The rate at which NCO burning occurs can be governed by the electron captures on ^{14}N (and hence the local density), but most of the energy production from the chain is supplied by the subsequent burning of ^{14}C . Once the right conditions are reached for electron captures onto ^{14}N , alpha captures occur on the freshly produced ^{14}C , releasing $Q = 6.227 \text{MeV}$ per ^{14}C consumed. At constant pressure and for ions strongly in

the liquid state, complete consumption of the ^{14}C at abundance $X_{14} \ll 1$ in a helium background leads to a temperature change of

$$\Delta T = \frac{2}{21} \frac{Q}{k_{\text{B}}} X_{14} \approx 7 \times 10^7 \text{ K} \left(\frac{X_{14}}{0.01} \right). \quad (1)$$

This entropy input is often large enough to trigger a full He burning runaway, and 3α burning quickly takes over as the dominant energy source once NCO has raised the temperature enough to initiate a runaway.

In contrast, when NCO reactions are ignored and ignition depends on 3α reactions alone, the models experience a later ignition in a different location. Helium burning via 3α is much more temperature sensitive than the electron captures that initiate the NCO chain, which depend primarily on the density. Despite previous work on mixing and viscous heating due to shear instabilities for white dwarfs accreting helium (Yoon & Langer 2004a; Yoon et al. 2004; Yoon & Langer 2004b), we ignore these effects in our models. Recent work by Piro (2015) suggests that this should be justified due to the baroclinic instability inhibiting development of shear instabilities at depths relevant for helium ignition.

3.1. Constant \dot{M} Without NCO

As a baseline for comparison, we first created a grid of WD models over a range of constant He accretion rates until they reached 3α ignition in their shells. During the accretion phase, the location of peak temperature lies outside the base of the accreted envelope due to the generic feature of a temperature inversion at these accretion rates, where electron conduction competes with the compressional heating by draining heat into the core and cooling the most dense inner layers of the envelope (Nomoto 1982). Since temperature inversions can cause a 3α based runaway to happen at a location in the accumulated material other than the base, the convective shell mass can be less than the total accreted mass. The top panel of Figure 4 shows the mass of the accumulated (solid) and convective (dashed) He shells at the moment of the instability triggered by the 3α reactions alone. The convective shell mass is defined here as all mass exterior to the location of the thermonuclear runaway, which will be swept up in the convection that occurs as a result of unstable ignition.

Models to the left of the solid point in Figure 4 accumulated sufficiently large He envelopes to achieve a density above $1.25 \times 10^6 \text{ g cm}^{-3}$ at the base of the He layer prior to 3α ignition, implying that for $\dot{M} < 4 \times 10^{-8} M_{\odot} \text{ yr}^{-1}$, the NCO reaction chain should provide extra heat near the dense base of the envelope. For all models accreting at constant \dot{M} , we assume an

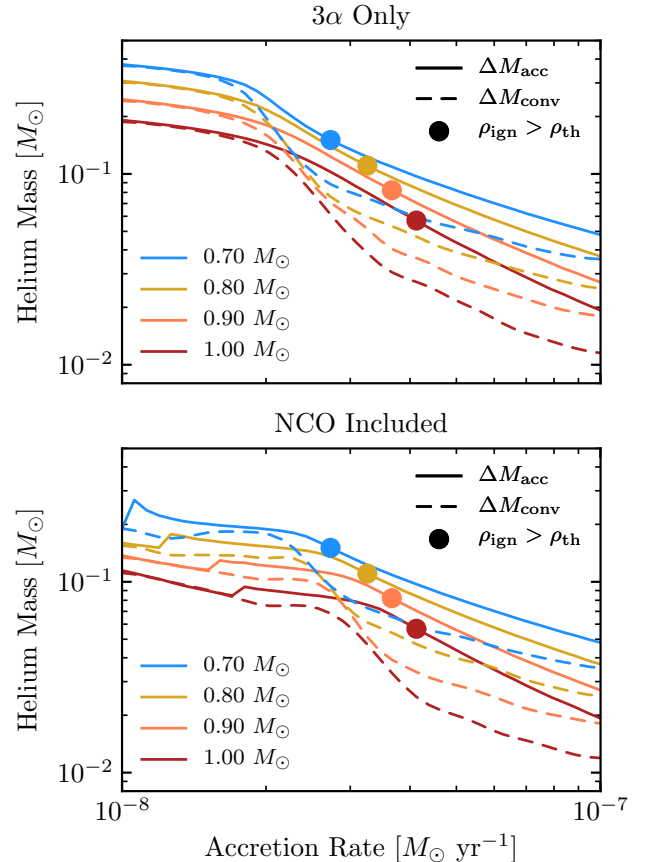


Figure 4. Accumulated helium shell masses and convective shell masses for flashes on various WD masses over a range of constant accretion rates. The upper panel shows flashes ignited by 3α alone, while the lower panel shows flashes when NCO reactions are included. Points indicate the first flash where the density at the base of the accreted material was above $\rho_{\text{th}} = 1.25 \times 10^6 \text{ g cm}^{-3}$.

initial core temperature of $T_c = 2 \times 10^7 \text{ K}$, appropriate for sdB+WD binary scenarios where the WD certainly has $10 - 100 \text{ Myr}$ to cool before the system makes contact. Lower core temperatures do not significantly impact the results.

3.2. Constant \dot{M} With NCO

A set of models similar to those shown in the top panel of Figure 4, but now including NCO reactions, is shown in the lower panel of Figure 4. For the region where density is beyond the threshold for NCO, we can see that the total accreted mass is somewhat lower due to earlier ignition, but in some cases the convective shell can still encompass more total mass due to the ignition occurring deeper in the accreted material.

The discontinuous feature in total accreted mass at low \dot{M} in the lower panel of Figure 4 is due to failed

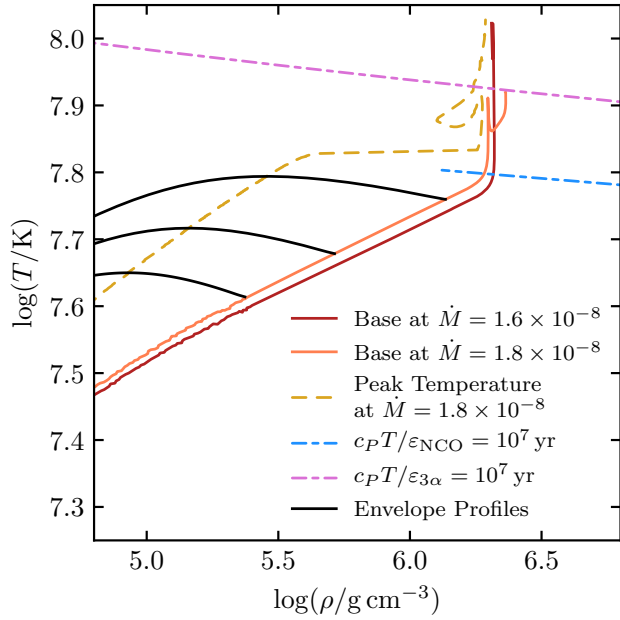


Figure 5. Density-temperature evolution of the accreted layer for a $1.0 M_{\odot}$ WD accreting at two different rates. These two models correspond to the discontinuity in the red line in the lower panel of Figure 4.

NCO ignitions for certain accretion rates. The finite supply of ^{14}C at $X_{14} \approx 0.01$ can be exhausted before NCO burning can fully ignite a 3α runaway. Due to the highly degenerate conditions at the base of He envelopes that are dense enough for NCO to occur, electron conduction can carry significant amounts of heat inward toward the cooler core as $^{14}\text{C}(\alpha, \gamma)^{18}\text{O}$ begins to run away. This leads to a ΔT smaller than that predicted by equation (1). Figure 5 shows the envelope $\rho - T$ evolution of two models at very similar \dot{M} , where one experiences a failed NCO runaway at its base before eventually experiencing a true 3α runaway at the peak temperature location further out in the accreted He envelope.

The metallicity sets the total amount of ^{14}N available for NCO reactions. Since ΔT from complete NCO consumption scales with X_{14} in equation (1), variation in metallicity directly corresponds to variation in the total thermal impact that NCO reactions can have. Varying only the initial ^{14}N content in the grid of constant \dot{M} models reveals a strong dependence on metallicity. These results are shown in Figure 6. For simplicity, we only present the variation in runs for the $0.7 M_{\odot}$ WD accretor model. Results for other accretor masses are similar. We assume that both the donor and accretor were born with the same metallicity, and that all CNO elements from the initial metallicity eventually end up as ^{14}N in both stars due to CNO burning in the evolu-

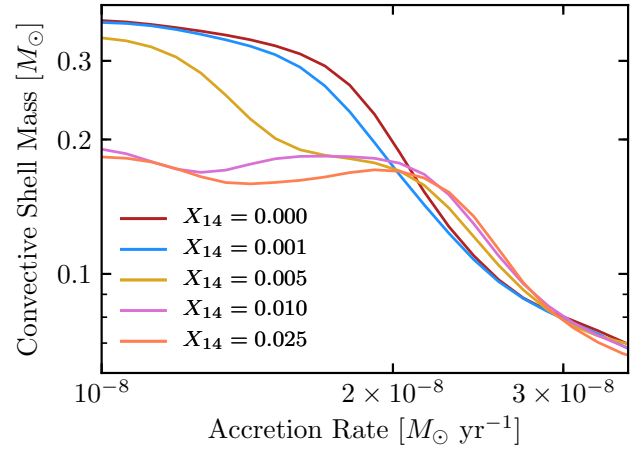


Figure 6. Convective shell masses at ignition as a function of constant accretion rate onto a $0.70 M_{\odot}$ WD for varying metallicity. The lines shown here for $X_{14} = 0.000$ and $X_{14} = 0.010$ correspond to the dashed blue lines in Figure 4.

tion that produces them. Hence the initial mass fraction of ^{14}N in the He envelope of the WD is correlated with that in the He accreted from the donor. Since the initial He envelope ends up as the base of the He layer after accretion, it contributes to the energy produced in the dense layers where NCO reactions occur.

Larger convective shell masses are associated with denser ignition locations that may be expected to experience dynamical burning. This provides the potential for developing detonation fronts that can give rise to interesting phenomenology such as .Ia supernovae (Bildsten et al. 2007; Shen & Bildsten 2009) or double detonation type Ia supernovae (Woosley & Weaver 1994) if the detonation can transition into the C/O core. The threshold envelope mass for dynamical burning is on the order of $\sim 0.1 M_{\odot}$. Because the NCO chain increases the convective shell mass in some regions, and the lower accretion rate regime is associated with large total accumulation masses, we see that NCO reactions are important for systems that have the potential to ignite dynamically.

Realistic binary systems often have accretion rates that vary across the boundary for high-density ignition shown by solid dots in Figure 4. Furthermore, Figure 4 shows that small variations in accretion rate around $2 - 4 \times 10^{-8} M_{\odot} \text{ yr}^{-1}$ can significantly impact the final convective shell mass, determining the dynamical fate of ignition. Clearly the constant \dot{M} approximation is a concern, so we now use the robust binary capabilities present in MESA to test a range of realistic parameters and scenarios for NCO ignitions.

4. REALISTIC MASS TRANSFER SCENARIOS

We now show that NCO burning plays a significant role in the initial flash encountered in He star or sdB donor systems when the WD builds up a large He envelope. Our results at constant \dot{M} in Section 3.2 suggest that the main impact of NCO reactions is to decrease both total accreted mass and convective envelope mass at low \dot{M} . However, our simulations of realistic binary evolution scenarios indicate that NCO burning can be much more significant than the constant \dot{M} results suggest. Neunteufel et al. (2016) studied systems like these using detailed binary evolution and accretion rates while drawing on Woosley & Kasen (2011) for ignition outcomes of WDs treated as point mass accretors. However, our results indicate that the constant \dot{M} results have limited predictive power in binary systems. Both the system and the WD must be evolved.

4.1. The First Flash after Contact

Brooks et al. (2015) used MESA’s binary evolution capabilities to model AM CVn systems, including realistic accretion histories for systems that are brought into contact by gravitational wave radiation, with self-consistent binary stellar evolution tracked through the accretion phase. Their study included many cycles of accretion, ignition, and flashes, but NCO reactions were not included. For many of the flashes, they found accumulated masses that were insufficient for the He layer to reach densities required for NCO reactions. A few of the flashes, however, did accumulate sufficient mass, particularly those occurring after the system first comes into contact and has not yet been warmed by previous flash episodes. In this section, we re-examine two of these binary scenarios where NCO reactions can play a role. The first is a $0.4 M_{\odot}$ He star donating onto a $0.8 M_{\odot}$ WD, and the second is the same donor model with a $1.0 M_{\odot}$ WD accretor. These correspond to panels 2 and 4 in figures 12 and 13 from Brooks et al. (2015).

The accretion rate is primarily governed by the physics of the donor star, and our study here leaves this unmodified, so we use the same \dot{M} histories as presented in figure 12 of Brooks et al. (2015) up to the point of ignition. With an identical starting model for the WD accretor and the accretion rate as specified by previous MESA binary runs, it is sufficient to follow the single star evolution in MESA for the accretor, with no further need to invoke MESA binary.

Figure 7 and Table 1 show that NCO reactions can modify the thermal structure prior to ignition, and more importantly, lead to ignition in the much deeper layers near the base of the accreted He. This effect is more pronounced for some systems than others, and the ac-

Table 1. Accreted and convective masses for the first helium flash

Accreted Mass (ΔM_{acc})	Without NCO	With NCO
$0.4 M_{\odot}$ He + $0.8 M_{\odot}$ WD	$0.107 M_{\odot}$	$0.107 M_{\odot}$
$0.4 M_{\odot}$ He + $1.0 M_{\odot}$ WD	$0.082 M_{\odot}$	$0.078 M_{\odot}$
CD -30° 11223	$0.175 M_{\odot}$	$0.163 M_{\odot}$
Convective Mass (ΔM_{conv})	Without NCO	With NCO
$0.4 M_{\odot}$ He + $0.8 M_{\odot}$ WD	$0.055 M_{\odot}$	$0.064 M_{\odot}$
$0.4 M_{\odot}$ He + $1.0 M_{\odot}$ WD	$0.039 M_{\odot}$	$0.054 M_{\odot}$
CD -30° 11223	$0.084 M_{\odot}$	$0.153 M_{\odot}$

cretion rate from binary evolution plays a large role in determining the thermal structure of the accreting WD, which governs the impact of NCO reactions. The accretion rate varies from $2 - 4 \times 10^{-8} M_{\odot} \text{ yr}^{-1}$ over the course of accumulation leading to the first flash (see e.g. figures 11 and 12 in Brooks et al. 2015). Since this \dot{M} range is precisely where Figure 4 shows the most significant variation in convective shell mass, there appears to be no reliable way to estimate the impact of NCO on ignition based on results at constant \dot{M} . Thus, accretion histories from full, self-consistent binary evolution such as those provided here need to be used to assess the condition at the time of thermal runaway.

4.2. The First Flash in CD -30° 11223

CD -30° 11223 (Geier et al. 2013) is a sdB+WD binary system with an orbital period of 70.5 minutes that will make contact in 40 Myr, likely while the sdB star’s core is still burning He. Brooks et al. (2015) used MESA to model the binary evolution of this system as a $0.510 M_{\odot}$ sdB star donating onto a $0.762 M_{\odot}$ WD, with initial conditions tuned to match the observations of Geier et al. (2013) assuming that the sdB star is just beginning helium core burning. They predicted that the WD would accumulate a large He envelope ($\Delta M_{\text{acc}} \approx 0.175 M_{\odot}$) which will then experience 3α ignition above the base of envelope, leading to a smaller convective envelope ($\Delta M_{\text{conv}} \approx 0.084 M_{\odot}$). For more information on the details of the modeling of this binary system, see section 3.2 in Brooks et al. (2015). Using the same accretion history and starting model, we modeled the evolution of the accreting WD both with and without NCO reactions. If we do not include the reactions necessary for the NCO chain in our network, our results match those described by Brooks et al. (2015). In contrast, with NCO burning included in the network, the extra heat injected in the

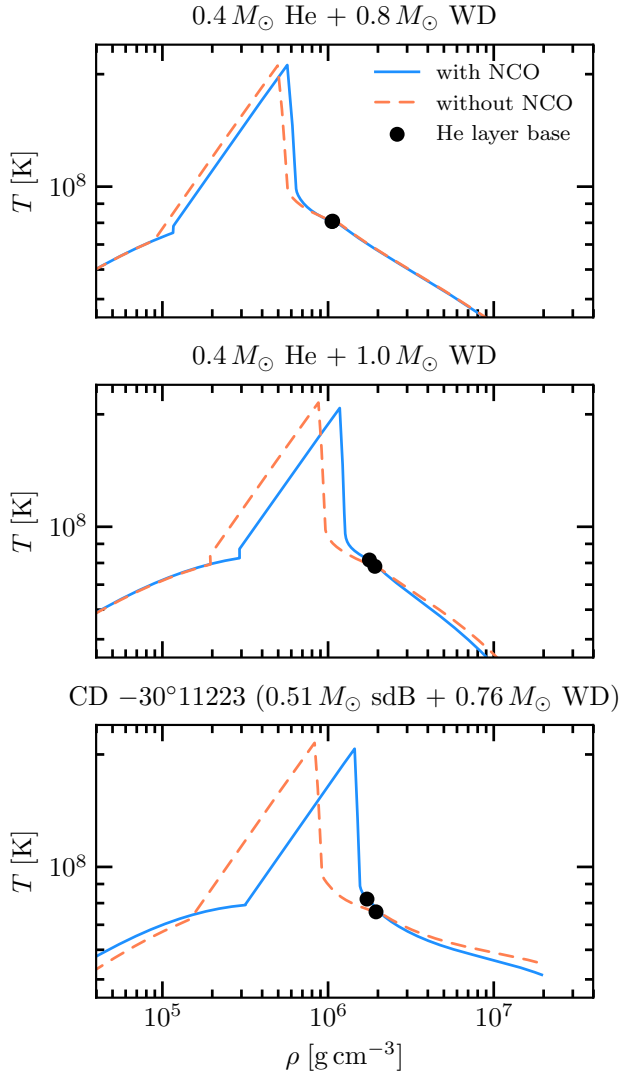


Figure 7. Profiles from models of the accreting WD in several binary systems after the flash has ignited. Models that include NCO reactions ignite in the deeper, denser region. In the case of CD $-30^\circ 11223$, the outer envelope has been noticeably warmed by additional heat from NCO burning prior to thermonuclear runaway.

deeper, denser layers of the envelope leads to an earlier ignition of a slightly smaller ($\Delta M_{\text{acc}} = 0.163 M_\odot$) He envelope triggered by ^{14}C . However, since the ignition is triggered much deeper in the accreted envelope, as seen in Figure 7, this results in a much larger, and more dynamically important, convective envelope of mass $\Delta M_{\text{conv}} = 0.153 M_\odot$.

This near doubling of the convective shell mass has no parallel from the results at constant \dot{M} shown in Section 3.2. In fact the trend seen there is in the opposite direction, where Figure 4 shows that NCO ignitions

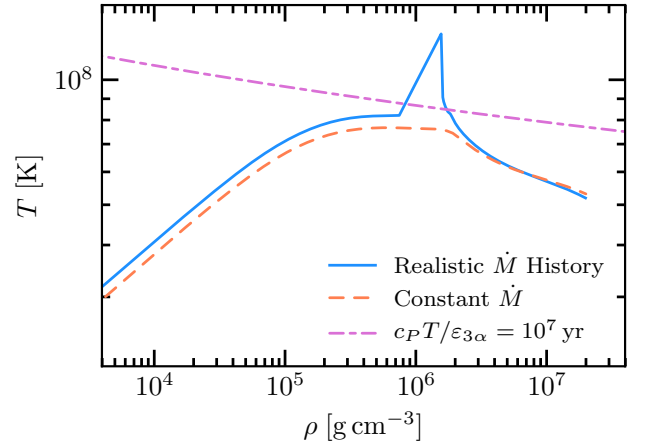


Figure 8. Effect of varying accretion history for CD $-30^\circ 11223$. The solid density-temperature profile shows the model evolved with a realistic accretion history from binary evolution. The dashed profile shows a model with a constant \dot{M} , corresponding to the time-average of the realistic history. The profiles are shown when the models reach a total mass of $M = 0.925 M_\odot$.

mostly tend to suppress the size of the convective shell by causing an earlier ignition while less total helium has had a chance to accumulate. This qualitatively different result of a much larger convective shell further motivates the use of full binary calculations in MESA to avoid the approximation of constant \dot{M} .

Figure 8 shows the contrast between modeling of CD $-30^\circ 11223$ including realistic accretion histories and modeling that makes the approximation of constant \dot{M} . The latter case assumes $\dot{M} = 1.93 \times 10^{-8} M_\odot \text{ yr}^{-1}$, the time-average of the accretion rate from the binary evolution calculations of Brooks et al. (2015). Both models here include the NCO reaction chain. After accumulating the same amount of mass to reach $M = 0.925 M_\odot$, the model with constant \dot{M} has not yet reached 3α ignition, while the realistic \dot{M} model has. Indeed, the constant \dot{M} model must accumulate 3% more mass before reaching ignition at a final mass of $M = 0.930 M_\odot$.

4.3. Metallicity and ^{14}N Abundance in sdB Donors

For sdB star donors, the interior abundance of ^{14}N may be somewhat lower due to burning during the helium core flash having processed some of the ^{14}N to ^{18}O and ^{22}Ne . MESA models of the helium core flash show about half of the ^{14}N in the interior of the He core will be consumed, leaving behind $X_{14} \approx 0.005$ of the original $X_{14} \approx 0.01$ for resulting sdB models (at solar metallicity). The abundance remains $X_{14} \approx 0.01$ only in the unprocessed outer $\sim 0.01 M_\odot$; see figure 42 of Paxton

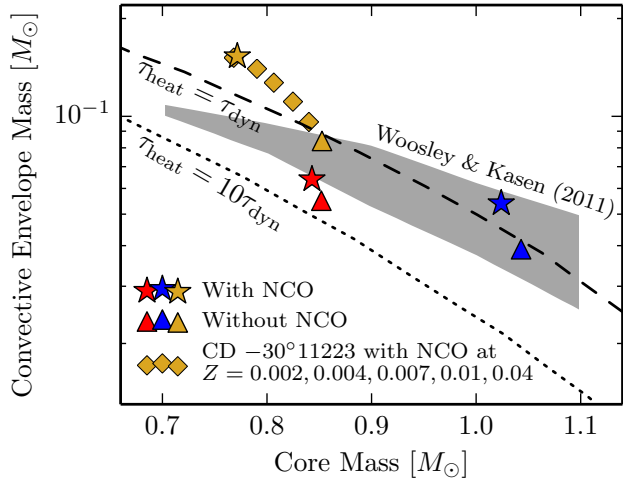


Figure 9. Masses from Table 1 showing that NCO burning pushes convective shells toward masses that will be more dynamical. Red points are for the $0.4 M_{\odot}$ He + $0.8 M_{\odot}$ WD system, and blue points are for the $0.4 M_{\odot}$ He + $1.0 M_{\odot}$ WD system. Gold points are for CD $-30^{\circ}11223$, with diamonds used to show models with metallicity other than solar. The grey shaded region shows the minimum allowed envelope masses for detonation or deflagration found by Woosley & Kasen (2011) for a range of core temperatures. Note that core mass in this figure is defined as all of the mass inside the convective shell.

et al. (2015). This means that after the first $0.01 M_{\odot}$ of material donated, the abundance of ^{14}N in the donated material will drop to $X_{14} \approx 0.005$. However, NCO reactions are primarily significant in material from the initial He envelope of the accretor and first donated material, which will eventually form the most dense region of the He layer at its base. As Table 1 shows, these NCO reactions at the base of the He layer can provide sufficient heating to ignite the envelope within $\approx 0.01 M_{\odot}$ of its base, so the lower abundance of ^{14}N in the accreted material further out should not significantly impact the outcome, and we ignore this change in abundance for all models presented in this work.

5. DYNAMICAL BURNING IN LARGE HELIUM ENVELOPES

Following Bildsten et al. (2007), we study the possibility of dynamical burning that may transition into a detonation by plotting the convective shell masses from Table 1 along with lines comparing the dynamic timescale to the heating timescale from burning in Figure 9. These timescales are defined as $\tau_{\text{dyn}} = H/c_{\text{sound}}$ and $\tau_{\text{heat}} = c_P T/\varepsilon_{\text{nuc}}$, where $H = P/\rho g$, and ε_{nuc} is dominated by 3α burning that takes over once the thermonuclear runaway is initiated. These quantities are

evaluated at the base of the convective burning shell. These lines are taken from figure 5 in Shen & Bildsten (2009). See also figure 7 in Brooks et al. (2015) for comparison, which has three points matching the three triangular symbols on our Figure 9, corresponding to binary models that did not include NCO reactions. For comparison, we also include the range of minimum allowed convective envelope masses for detonation or deflagration found by Woosley & Kasen (2011) in their extensive grid of constant \dot{M} models.

The solar metallicity model for CD $-30^{\circ}11223$ (gold star in Figure 9) is likely to reach especially dynamical burning conditions. At 0.1 s before the most rapid evolution occurs in the MESA model, τ_{heat} becomes shorter than τ_{dyn} . If allowed to evolve beyond that point, peak burning reaches $\tau_{\text{heat}} \approx 0.1\tau_{\text{dyn}}$, and convective velocities reach nearly the sound speed. We expect that a detonation should develop around this point, but hydrostatic 1D MESA calculations are not reliable for evolution beyond this point. For more detailed study of the conditions of dynamical burning and convection leading to potential ignition of a detonation, see the recent work of Jacobs et al. (2016). The outcomes of their 3D hydrodynamical simulations appear to be broadly consistent with our expectations based on Figure 9, but further study is warranted.

The models for binary systems described in Sections 4.1 and 4.2 assumed solar metallicity for both the donor star and the WD progenitor, but the metallicity of CD $-30^{\circ}11223$ is not known. Varying the metallicity of the system changes the amount of time necessary for the NCO chain to deposit enough heat to initiate a runaway, and hence the metallicity influences both total accreted mass and convective shell mass. This trend is clear in the diamond symbols showing convective shell masses in Figure 9, which represent the binary system described in Section 4.2 modeled with NCO reactions over a range of metallicities. For $Z \lesssim 0.02$, there is a continuous progression toward larger convective shell masses as metallicity increases for this system. However, once $Z \gtrsim 0.02$, there is plenty of ^{14}N present for the NCO chain to ignite runaway burning quickly after electron captures get underway past the threshold density, and hence higher metallicity does not significantly change the burning outcome past this point of saturation around solar metallicity.

6. CONCLUSIONS AND FUTURE WORK

Our results show that NCO reactions play an important role in triggering envelope ignitions for WDs accreting He at rates in the range $1 - 5 \times 10^{-8} M_{\odot}/\text{yr}$. Binary systems composed of an sdB star donating He

onto a WD naturally give rise to accretion rates that vary within this range. Because the thermal time is comparable to the accretion time in these He envelopes, it is necessary to model systems in a way that consistently tracks both the full accretion rate history and the evolution of the WD in response. Extrapolations from results using constant accretion rates are inadequate.

Though studies at constant \dot{M} have concluded that NCO reactions provide only minor corrections with no qualitative differences, binary evolution with \dot{M} that varies over the accumulation phase shows that NCO can be more important than previously thought. Models for the observed system CD $-30^{\circ}11223$ illustrate the most pronounced qualitative differences that can arise as a result of NCO triggered ignitions during binary evolution, with a convective envelope mass that is twice as large in the case that includes NCO reactions. The recent discovery by Kupfer et al. (2017) of another system with a tight (87 min) sdB+WD binary demonstrates that detailed binary modeling with NCO reactions will continue to remain important as more of these systems are discovered.

The dynamical nature of the most extreme flashes presented here suggests that NCO triggered ignitions can lead to He detonations. We have also found that metallicity is directly correlated with the potential outcomes in these systems, with solar metallicity progenitors providing ample fuel for the NCO chain, while lower metallicities predictably soften its effects. Helium shell detonations are still possible in low metallicity environments without NCO triggers, but they appear less likely according to Figure 9. Though we have not exhaustively studied this trend, it may suggest a correlation between higher metallicity environments and observations involving events with thick helium shell detonations.

Future exploration should include modeling of additional variables that can impact the binary evolution of sdB+WD systems. Models presented here assumed that the sdB star in CD $-30^{\circ}11223$ is at the beginning of core He burning, but this age is not constrained. If the sdB

star has a different He core burning age, the system will make contact at a different stage of the sdB life cycle, and the resulting accretion rate will vary accordingly. Since our results here show that the details of the accretion rate are crucial, variations in the \dot{M} predicted by binary evolution may lead to different results for the total convective shell mass ignited on the WD. We anticipate a potential variation of predicted outcomes for the final fate of any given system where the sdB star age is not known.

More work is also necessary to strengthen our understanding of evolution beyond the onset of dynamical burning. Understanding the transition into detonation and the resulting effects on both the envelope and core will be crucial for making a specific prediction about the ultimate observable nature of these NCO triggered events.

We thank Jared Brooks for many helpful discussions on use of the binary capabilities in MESA for modeling AM CVn systems and for providing accretion rate histories from his binary results. We thank Bill Wolf for developing excellent tools for scripting the many MESA runs that went into Section 3, as well as helping plot the results. We thank Gabriel Martínez-Pinedo for providing a machine readable version of the $^{14}\text{N}(e^-, \nu)^{14}\text{C}$ rate and for helpful communications regarding matrix elements. We thank Hendrik Schatz for helpful discussions regarding the $^{14}\text{C}(\alpha, \gamma)^{18}\text{O}$ rate. Support for this work was provided by NASA through Hubble Fellowship grant # HST-HF2-51382.001-A awarded by the Space Telescope Science Institute, which is operated by the Association of Universities for Research in Astronomy, Inc., for NASA, under contract NAS5-26555. This work was supported by the National Science Foundation under grants PHY 11-25915 and ACI 13-39581. This research is funded in part by the Gordon and Betty Moore Foundation through Grant GBMF5076 to L.B..

Software: MESA (Paxton et al. 2011, 2013, 2015, 2016), Matplotlib (Hunter 2007), Numpy (van der Walt et al. 2011), MesaScript (Wolf et al. 2017)

REFERENCES

- Ajzenberg-Selove, F. 1991, Nuclear Physics A, 523, 1
- Bildsten, L., Shen, K. J., Weinberg, N. N., & Nelemans, G. 2007, ApJL, 662, L95
- Brooks, J., Bildsten, L., Marchant, P., & Paxton, B. 2015, ApJ, 807, 74
- Cyburt, R. H., Amthor, A. M., Ferguson, R., et al. 2010, ApJS, 189, 240
- Fuller, G. M., Fowler, W. A., & Newman, M. J. 1980, ApJS, 42, 447
- . 1985, ApJ, 293, 1
- Geier, S., Marsh, T. R., Wang, B., et al. 2013, A&A, 554, A54
- Hashimoto, M. A., Nomoto, K. I., Arai, K., & Kaminisi, K. 1986, ApJ, 307, 687

- Hunter, J. D. 2007, *Computing In Science & Engineering*, 9, 90. <https://doi.org/10.5281/zenodo.248351>
- Iben, I., Nomoto, K., Tornambe, A., & Tutukov, A. V. 1987, *ApJ*, 317, 717
- Iliadis, C., Longland, R., Champagne, A. E., Coc, A., & Fitzgerald, R. 2010, *Nuclear Physics A*, 841, 31
- Jacobs, A. M., Zingale, M., Nonaka, A., Almgren, A. S., & Bell, J. B. 2016, *ApJ*, 827, 84
- Johnson, E. D., Rogachev, G. V., Mitchell, J., Miller, L., & Kemper, K. W. 2009, *PhRvC*, 80, 045805
- Kupfer, T., van Roestel, J., Brooks, J., et al. 2017, *ApJ*, 835, 131
- Martínez-Rodríguez, H., Piro, A. L., Schwab, J., & Badenes, C. 2016, *ApJ*, 825, 57
- Nelemans, G., Yungelson, L. R., & Portegies Zwart, S. F. 2004, *MNRAS*, 349, 181
- Neunteufel, P., Yoon, S.-C., & Langer, N. 2016, *A&A*, 589, A43
- Nomoto, K. 1982, *ApJ*, 253, 798
- Paxton, B., Bildsten, L., Dotter, A., et al. 2011, *ApJS*, 192, 3
- Paxton, B., Cantiello, M., Arras, P., et al. 2013, *ApJS*, 208, 4
- Paxton, B., Marchant, P., Schwab, J., et al. 2015, *ApJS*, 220, 15
- Paxton, B., Marchant, P., Schwab, J., et al. 2016, *ApJS*, 223, 18
- Piersanti, L., Cassisi, S., & Tornambé, A. 2001, *ApJ*, 558, 916
- Piro, A. L. 2015, *ApJ*, 801, 137
- Potekhin, A. Y., Chabrier, G., & Rogers, F. J. 2009, *PhRvE*, 79, 016411
- Schwab, J., Quataert, E., & Bildsten, L. 2015, *MNRAS*, 453, 1910
- Schwab, J., Quataert, E., & Bildsten, L. 2016, *MNRAS*, 458, 3613
- Shen, K. J., & Bildsten, L. 2009, *ApJ*, 699, 1365
- . 2014, *ApJ*, 785, 61
- van der Walt, S., Colbert, S. C., & Varoquaux, G. 2011, *Computing in Science & Engineering*, 13, 22. <https://pypi.python.org/pypi/numpy/1.12.1>
- Wolf, B., Bauer, E. B., & Schwab, J. 2017, *wmwolf/MesaScript: A DSL for Writing MESA Inlists*, v1.0.2, Zenodo, doi:10.5281/zenodo.826954. <https://doi.org/10.5281/zenodo.826954>
- Woosley, S. E., & Kasen, D. 2011, *ApJ*, 734, 38
- Woosley, S. E., & Weaver, T. A. 1994, *ApJ*, 423, 371
- Yoon, S.-C., & Langer, N. 2004a, *A&A*, 419, 645
- . 2004b, *A&A*, 419, 623
- Yoon, S.-C., Langer, N., & Scheithauer, S. 2004, *A&A*, 425, 217